Article

Microstructure and Mechanical–Tribological Properties of HVOF-Sprayed (WC–Co+Ni) Coatings on Ductile Cast Iron

Marzanna Ksiazek * , Lukasz Boron , Adam Tchorz

Posted Date: 3 April 2026

doi: 10.20944/preprints202604.0209.v1

Keywords: HVOF; WC–Co coatings; Ni addition; microstructure; wear resistance; adhesion; tribology

 doi:10.20944/preprints202604.0209.v1

Article

Microstructure and Mechanical–Tribological Properties of HVOF-Sprayed (WC–Co+Ni) Coatings on Ductile Cast Iron

Marzanna Ksiazek [1,*], Lukasz Boron [2] and Adam Tchorz [2]

[1] AGH University of Krakow, Department of Non-Ferrous Metals, al. A. Mickiewicza 30, 30-059 Krakow, Poland

[2] Lukasiewicz Research Network-Krakow Institute of Technology, 73 Zakopianska Str., 30-418 Krakow, Polan

* Correspondence: mksiazek@agh.edu.pl; Tel.: +48-12-617-38-81

Abstract

High Velocity Oxy-Fuel (HVOF) thermal spraying is widely used for the deposition of dense coatings with low porosity, high hardness, and superior fracture resistance. Tungsten carbide–cobalt (WC–Co) coatings are extensively employed in industrial and aerospace applications due to their excellent wear resistance and mechanical performance; however, further improvement in crack resistance and adhesion remains a key challenge. In this study, WC–Co+Ni composite coatings were deposited on ductile cast iron by HVOF, with particular emphasis on the role of Ni particle addition in tailoring coating microstructure and performance. Microstructural characterization was carried out using light, scanning, and transmission electron microscopy (LM, SEM, TEM), while phase composition and chemical analysis were determined by X-ray diffraction (XRD) and energy-dispersive spectroscopy (EDS). The coatings exhibited a dense, low-porosity microstructure composed of partially molten Ni particles and fine WC and W_2C carbides embedded in a cobalt-based matrix, with locally nanocrystalline features. XRD analysis confirmed WC and W_2C as the dominant phases, with weak reflections indicating the possible formation of the η-phase (Co_6W_6C). Mechanical and tribological performance, evaluated by instrumented indentation and scratch testing, showed that Ni addition significantly enhances crack resistance, wear resistance, and coating–substrate adhesion. The results demonstrate that Ni-modified WC–Co coatings deposited by HVOF enable effective microstructural design, leading to improved durability and performance, which makes them promising candidates for advanced coating applications.

Keywords: HVOF; WC–Co coatings; Ni addition; microstructure; wear resistance; adhesion; tribology

1. Introduction

Tungsten carbide–cobalt (WC–Co) composite coatings are among the most widely used protective materials in surface engineering due to their exceptional resistance to abrasive and erosive wear. Their performance arises from the synergistic combination of extremely hard WC particles and a relatively ductile cobalt binder phase, providing an optimal balance of hardness, fracture toughness, and load-bearing capacity. Consequently, WC–Co coatings are extensively applied in demanding industrial environments, including cutting and forming tools, casting molds, mining equipment, and mechanical components exposed to severe contact stresses and impact loads [1–4].

Among the available deposition techniques for carbide-based coatings, High Velocity Oxy-Fuel (HVOF) thermal spraying is widely used to produce dense and mechanically robust coatings. In this process, powder particles are accelerated to supersonic velocities in a high-temperature combustion jet and impact the substrate in a semi-molten state. Rapid splat deformation and solidification result in a lamellar microstructure with low porosity and strong intersplat cohesion [5–8]. Compared with

 doi:10.20944/preprints202604.0209.v1

conventional plasma spraying, HVOF deposition limits excessive carbide dissolution and decarburization while maintaining high coating density and mechanical integrity [6,9]. The final properties of the coatings are strongly influenced by processing parameters such as particle velocity, temperature, spray distance, and carrier gas pressure, which govern microstructure, porosity, and residual stress [7,10].

During HVOF deposition, complex thermochemical reactions can occur within the particle stream and during splat solidification, often resulting in partial decarburization of WC and the formation of secondary phases such as W_2C and η-phase carbides (e.g., Co_6W_6C). The presence and distribution of these phases significantly affect coating hardness, elastic modulus, and fracture resistance [12–15]. While moderate phase transformation can enhance hardness and abrasion resistance, excessive formation of brittle phases may reduce fracture toughness and accelerate coating degradation under cyclic or impact loading [9,14,16]. Therefore, controlling phase evolution during thermal spraying remains a critical challenge in developing high-performance WC-based coatings.

Recent studies have explored the modification of WC–Co feedstock powders through the incorporation of metallic alloying elements such as Ni, Cr, Al, and complex alloys to improve coating performance. Alloying primarily affects the metallic binder phase, increasing its ductility, facilitating stress relaxation during rapid solidification, and enhancing intersplat cohesion [17–19]. Moreover, suitable alloying strategies can suppress excessive WC decarburization, limit the formation of undesirable secondary phases, and promote a more homogeneous distribution of the binder phase within the lamellar structure [18,20]. These microstructural modifications can alter wear mechanisms, shifting the dominant response from brittle carbide pull-out toward matrix-controlled plastic deformation, thereby improving wear resistance and coating durability [16,21].

Nickel additions have received particular attention due to their beneficial influence on coating integrity and mechanical stability. Ni-containing matrices exhibit increased ductility and energy absorption during deformation, which reduces microcracking and limits carbide fragmentation under tribological loading [23–25]. Similar improvements have been observed with chromium additions, which stabilize the carbide–matrix interface, reduce porosity, and increase coating hardness, enhancing resistance to wear and erosion [26,27]. Additionally, grain-growth inhibitors such as VC, Cr_3C_2, TiC, and NbC can suppress carbide coarsening and promote microstructural refinement, leading to improved mechanical stability and coating durability [28–30].

The microstructure of HVOF-sprayed WC–Co coatings is governed by rapid thermomechanical interactions involving partial particle melting, splat deformation, and solidification. These processes produce a lamellar structure composed of WC/W_2C particles embedded in a metallic matrix, which may include nanoscale or amorphous regions [10,31]. The size, morphology, and spatial distribution of carbide particles play an important role in determining hardness, fracture toughness, and tribological behavior [14,18,32]. Furthermore, tribochemical reactions during sliding contact may form protective tribofilms that influence friction and wear resistance, directly linking microstructural features with operational performance [22,33].

Ductile cast iron is commonly used as a substrate material due to its favorable mechanical strength, good machinability, and thermal compatibility with carbide coatings. However, coating durability strongly depends on the integrity of the coating–substrate interface, including interfacial adhesion, residual stress distribution, and microstructural continuity [5,14].

In this context, the present study aims to modify the chemical composition of WC–12Co powders by incorporating nickel particles and to deposit the resulting coatings on ductile cast iron using the HVOF process. Particular attention is paid to the effect of this modification on the microstructure and the mechanical and tribological properties of the coatings.

 doi:10.20944/preprints202604.0209.v1

2. Materials and Methods

2.1. Preparating of Coating

Coating: WC-Co+Ni was applied by supersonic flame spraying of carbide powder containing WC-12Co (88 wt% WC-12 wt% Co) of grain size -45+5 μm, (Diamalloy 2002 Salzer-Metco, Pfattikon, Switzerland) onto a ductile iron substrate. The WC-Co+Ni composite coating was obtained by introducing 10% of 20 μm Ni particles into the carbide powder. The powder mixture used to produce the composite coating consisted of 79.2 wt.% WC, 10.8 wt.% Co and 10.0 wt.% Ni. The HV-50 HVOF System supersonic spraying system at Plasma System S.A. (Siemianowice, Silesia, Poland) was used for spraying the coatings, in which a mixture of aviation kerosene and oxygen was used as fuel for the spraying process. Coating application parameters are listed in Tab. 1. Substrate made of EN-GJS-500-7 ductile iron with the following chemical composition: 3.61% C, 2.29% Si, 0.45% Mn, 0.045% P, 0.009% S, 0.03% Cr, 0.01% Ni, 0.057% Mg, 0.75% Cu, and the rest Fe, (in weight percentage), and was characterised by the following mechanical properties: Y.S = 340 (MPa) T.S = 500 (MPa), Elongation = 7%, Hardness = 220HB. The substrate samples had dimensions of 100 x 15 x 5 mm^3. Before spraying, the surface of the substrates has been treated with a loose corundum of 20 mesh granulation to improve the mechanical adhesion of coatings. The substrate surface roughness parameter R_a was 30 μm. The average coating thickness was 280 μm.

Table 1. HVOF spraying parameters of as sprayed WC-Co+Ni coatings.

Gun Movement Speed (mm/s)	Oxygen (l/min)	Kerosene (l/h)	Powder Feed Rate (g/min)	Powder Feed Gas (l/min)	Spraying Distance (mm)
583	944	25.5	92	Nitrogen, 9.5	370

2.2. Microstructure Characterization

A light microscope (LM) Axio Observer Zm1 by Zeiss, a scanning electron microscope (SEM) Dual Beam Scios FEI, and a transmission microscope (TEM, JOEL 2010 ARD) equipped with EDS spectrometers were used to study the microstructure and chemical composition of the coating/substrate system. Preparations of the coating/substrate type for the transmission microscope in the form of a thin film were obtained by using ion thinning in a special device, the Gatan PIPS691V3.1 (Pleaasanton, USA) for low-angle thinning [34]. Phase composition studies were carried out on the X'Pert Pro Panalytical Diffractometer in the angular range of 20-90º with CuK radiation. After such measurements, the obtained spectra were subjected to preliminary numerical processing using the "EVA" software, consisting of cutting off the background and reducing noise using the Furier transform. Phase identification was carried out with the help of the ICDD database. Based on Rietveld analysis of XRD data with the use of GSAS/EXPGUI, a set of software phase compositions were derived. The average crystallite size was calculated from the Scherrer formula after taking into account the instrumental broadening. The porosity of the carbide coating was evaluated using X-ray computed tomography (XCT) on a Phoenix Nanotom nanotomograph (GE Sensing & Inspection Technologies) with AxioVision image analysis software. Measurements were conducted on 10 regions of the coating using cuboid-shaped coating/substrate samples of approximately 2 mm in size (Figure 1).

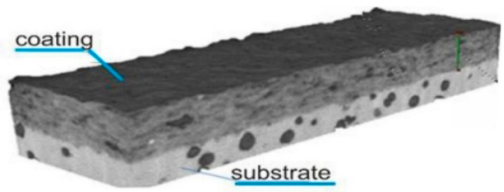

Figure 1. Cuboid-shaped coating/substrate sample (~2 mm) used for XCT analysis.

 doi:10.20944/preprints202604.0209.v1

Studies of the surface topography of the coatings and the determination of the surface roughness parameters R_a (average roughness value) and R_z (average roughness height) were carried out using a LEXT OLS4100 laser confocal microscope from OLYMPUS. Three measurement lines of coating surface roughness were used to calculate the parameters for each type of coating. Three-dimensional images and their analysis allowed for precise recognition of the geometric structure of the tested surfaces.

2.3. Mechanical and Tribological Properties

Studies of mechanical properties, which included indantation measurements of hardness (H_{IT}), Young's modulus of elastisity (E_{IT}), and fracture toughness (K_{IC}), were carried out on the multifunctional measurement platform Micro Combi Tester of Swiss Company CSM Instruments. H_{IT}, E_{IT}, and K_{IC} were determined by sample indentation (cross-section of coating/substrate samples) using a Vickers diamond indenter. Measurements continuously recorded the load and depth of penetration of the indenterring the loading and unloading cycles. The maximum load value for the hardness measurement and the Young module was 1 N, the load and unload speed was 2 N/min, the maximum load maintenance time was 10 s, and the contact force was 0.03 N. For The analysis of micromechanical properties was based on the Oliver and Pharr method, according to which the hardness (H_{IT}) and Young's modulus of elasticity (E_{IT}) were calculated from the penetration curve (Figure 2). The measurement of the microhardness was done by a matrix distribution consisting of 15 measuring points on the cross-section of the coating for each coating/substrate system (Figure 2). The measurement positions along one measuring line: I, II, II, IV, and V were precisely defined with the special "Visual Advanced Matrix" module thanks to the integrated light microscope.

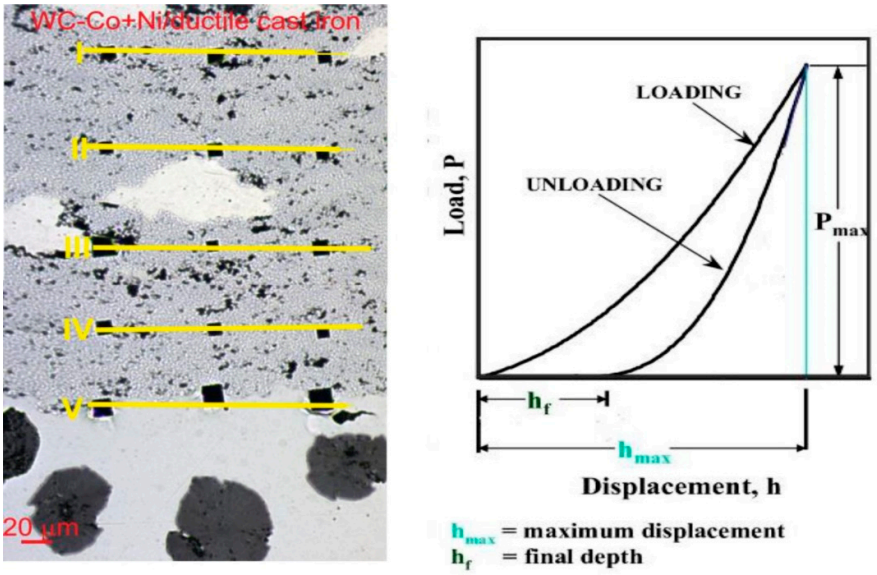

Figure 2. Measurement of microhardness (H_{IT}) by matrix distribution on the cross-section of the coating and typical relationship between load and displacement during indentation.

Indentation fracture toughness was determined by the K_{IC} parameter, i.e., the critical value of the stress intensity coefficient, by direct measurement of the length of cracks that appeared in the corners as a result of the penetration of a Vickers indenter under the influence of a given load: 5, 10, 15, and 20 N (the speed of loading and unloading was 40 N/min, maximum load holding time was 10 s, and contact load was 0.03 N). For this purpose, the lengths of the cracks and the lengths of the indentation diagonals were determined using an integrated light microscope (Figure 3). Three indentations were made in each coating/substrate type sample at a given load. After determining the

 doi:10.20944/preprints202604.0209.v1

total length of the cracks, the type of cracks was identified, taking into account the length ratio l/a. When the l/a ratio is > 1.5, the Anstis formula [35] is used. To determine the fracture toughness, take into account two parameters: the load (P) and the length of the crack (l).

Anstis formula:

$$K_{IC} = 0{,}016 \cdot \left(\frac{E}{HV}\right)^{0.5} \cdot \frac{P}{c^{1,5}} \quad (1)$$

where K_{IC} – fracture toughness coefficient, P – indenter load [N], HV - Vickers hardness, E – Young's modulus of elasticity [MPa], c= a+l – length of half of the indent's diagonal + length of the crack initated from corner of Vickers indent [m], a – length of half of the indent's diagonal [μm], l - length of the crack initated from corner of Vickers indent [μm].

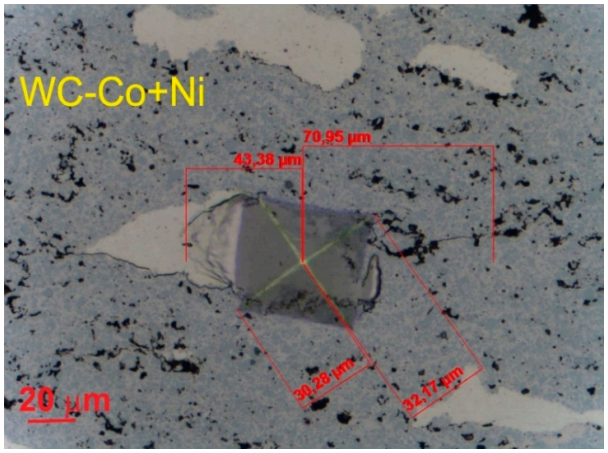

Figure 3. Scheme for measuring indentation fracture toughness (K_{IC}) in the WC-Co+Ni coating.

The strength of the coating/substrate joint was evaluated using a four-point bending test performed on an INSTRON 8800M testing machine. A specially designed fixture was used for specimens with dimensions of 36×13×3 mm³. The support span was 25 mm, and the crosshead displacement rate was set to 1 mm/min. For each test condition, three specimens were examined. After the bending tests, fracture surfaces were analyzed using scanning electron microscopy (SEM).

The bending strength was calculated according to the formula:

$$\sigma = \frac{3}{2} \cdot F_f \frac{l}{d \cdot h^2} \quad (2)$$

where σ - bending strength [MPa] F_f - destructive force [N], l - load spacing [mm], d – witdh of the specimen [mm], h - height of the specimen [mm].

Tests of adhesion of coatings to the substrate and determination of other mechanical types of damage, such as depth of penetration of the indenter, cracks, and the beginning of delamination in the crack profile of the scratch path, were carried out using a scratch test using a Rockwell C-type diamond indenter with a radius of curvature of 100 μm with a penetrator force of 5, 10, 15, 20, and 25 N, using a multifunction measuring platform (Micro-Combi Tester, Switzerland) equipped with Anton Paar scratch test heads according to the standard [36]. The tests were carried out on the cross-sectioned samples embedded in Durofast hard epoxy resin and then polished using standard metallographic procedures. The scratch test was performed under a constant load, with the indenter moving from the substrate through the coating into the resin in which the sample was embedded. The scratch lengths were 1.2 mm and 2.4 mm, and the indenter speed was 0.4 mm/min. Failure of the coating/substrate system was detected and evaluated by examining the resulting scratch using lightl microscopy (LM) and scanning electron microscopy (SEM). Furthermore, the projected area of the cone-shaped fracture within the coating was determined after the scratch test as $A_{cn}=L_x \times L_y$ (Figure 4). For the constant load condition, this parameter was used to assess coating cohesion and wear resistance, based on measurements performed using a light microscope.

 doi:10.20944/preprints202604.0209.v1

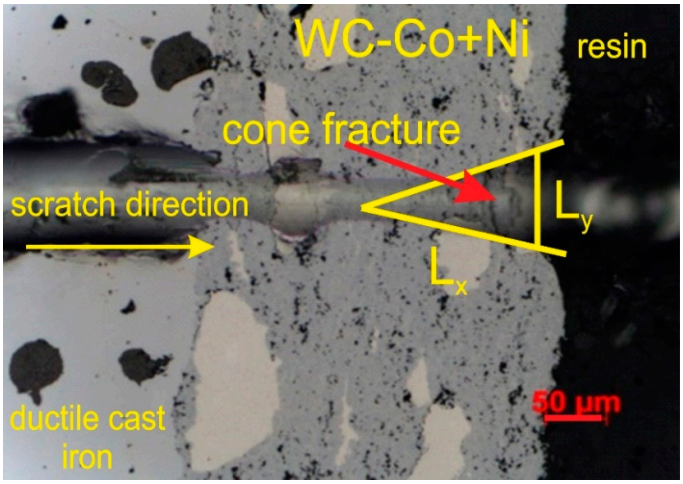

Figure 4. An example image of a scratch track in the substrate/coating/resin system. (F=10 N).

The abrasive wear resistance of ductile cast iron and the WC-Co+Ni/ductile cast iron coating system was evaluated using a ball-on-disc tribometer (ELBIT, Poland) at ambient temperature. Tests were conducted for 1000 s under a normal load of 25 N and a rotational speed of 3500 rpm. The tribological pair consisted of a stationary sample plate and an Al_2O_3 ball (radius 0.6 mm, diameter 1.2 mm) as the counterbody, moving along a circular track with a radius of 5 mm. The sample was pressed against the ball with a constant, precisely controlled normal force, while the counterbody was mounted on a rigid fixture to ensure stable contact. Friction force, sliding distance, rotational speed, contact temperature, wear depth, and wear rate were continuously recorded using dedicated software. Linear wear of the sample was measured with a high-precision displacement sensor. Post-test analyses of wear track morphology and elemental composition were performed to identify dominant wear mechanisms and the nature of tribological interactions.

3. Results and Discussion

3.1. Microstructure and Phase Composition of the (WC–Co+Ni)/Ductile Cast Iron System

The microstructure of the composite (WC–Co+Ni) coating deposited on ductile cast iron, observed by light microscopy (Figure 5), exhibits a typical lamellar morphology characteristic of HVOF-sprayed coatings. It consists of flattened splats formed as a result of particle impact and severe plastic deformation upon collision with the substrate. Fine WC particles are relatively uniformly distributed within the cobalt-based binder matrix, contributing to the structural homogeneity of the coating. The microstructure also reveals the presence of larger, highly deformed metallic regions corresponding to nickel particles, which underwent partial or complete melting during the spraying process (Figure 5). These Ni-rich regions form continuous metallic bridges between lamellae, enhancing interlamellar cohesion and improving overall ductility. As commonly observed in thermally sprayed composite systems, the low-melting metallic phase exhibits a higher degree of plastic deformation and effectively fills interlamellar voids between carbide particles. As a result, the coating exhibits a dense and compact structure with a low level of defects. It is characterized by low, isolated porosity, quantified as 3.2 ± 0.6% based on tomographic analysis, as well as a limited presence of oxides, mainly in the form of thin layers at lamellar boundaries. The coating–substrate interface is continuous and well developed, with no evidence of substrate melting, indicating that mechanical interlocking is the dominant adhesion mechanism in the HVOF process. The addition of Ni plays a key role in microstructural development by enhancing particle plasticization and promoting pore filling, thereby improving interlamellar cohesion and reducing structural defects. Consequently, the coating exhibits a high degree of densification, strong adhesion to the substrate, and a well-balanced distribution of hard ceramic and metallic phases. The presence of the ductile Ni phase contributes to

 doi:10.20944/preprints202604.0209.v1

enhanced stress accommodation, improved crack resistance, and increased overall coating toughness, which is particularly beneficial under mechanical loading conditions typical for tribological applications.

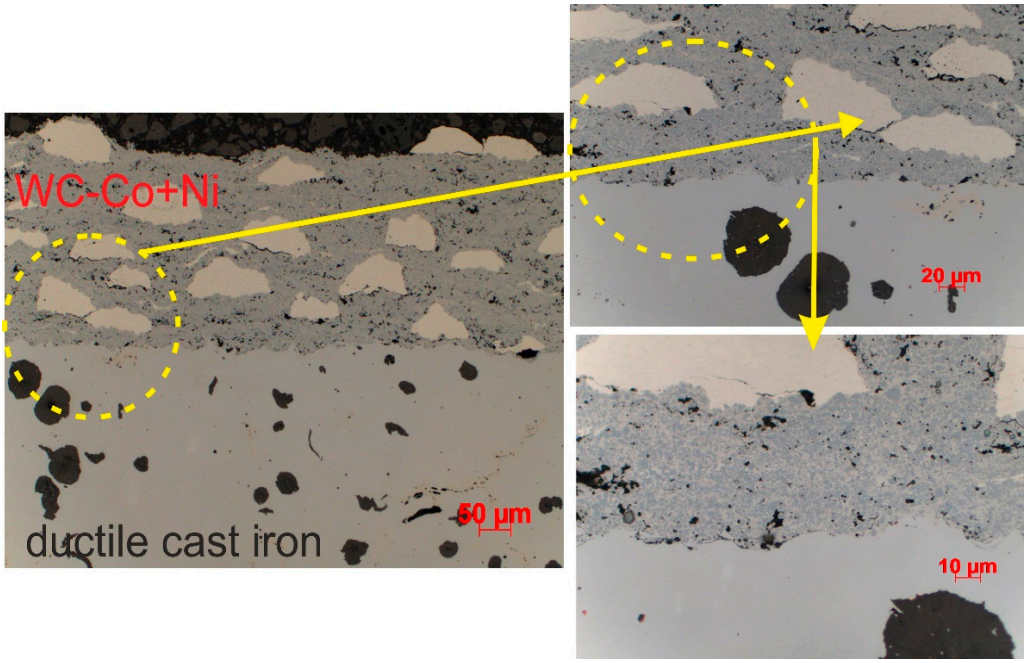

Figure 5. Microstructure of the (WC-Co+Ni/)ductile cast iron system at low and high magnification.

Observations performed using scanning electron microscopy (SEM), supported by energy-dispersive X-ray spectroscopy (EDS), revealed significant refinement of tungsten carbide particles from an initial size of approximately 40 µm to 0.5–2.5 µm after the spraying process (Figure 6). This refinement was observed both within the coating bulk and in the vicinity of the coating–substrate interface. EDS analysis confirmed the presence of elements characteristic of both the coating and the substrate, while elemental mapping revealed distinct concentration gradients across the interface. Transmission electron microscopy (TEM) investigations of thin regions of the (WC–Co+Ni) coating revealed a nanocrystalline microstructure with a banded morphology (Figure 7). The observed parallel bands, with thicknesses in the range of approximately 100–300 nm, indicate pronounced phase refinement and preferential alignment along the spray direction. Such a microstructure is conducive to increased hardness and improved tribological performance, while maintaining a high degree of interfacial cohesion.

 doi:10.20944/preprints202604.0209.v1

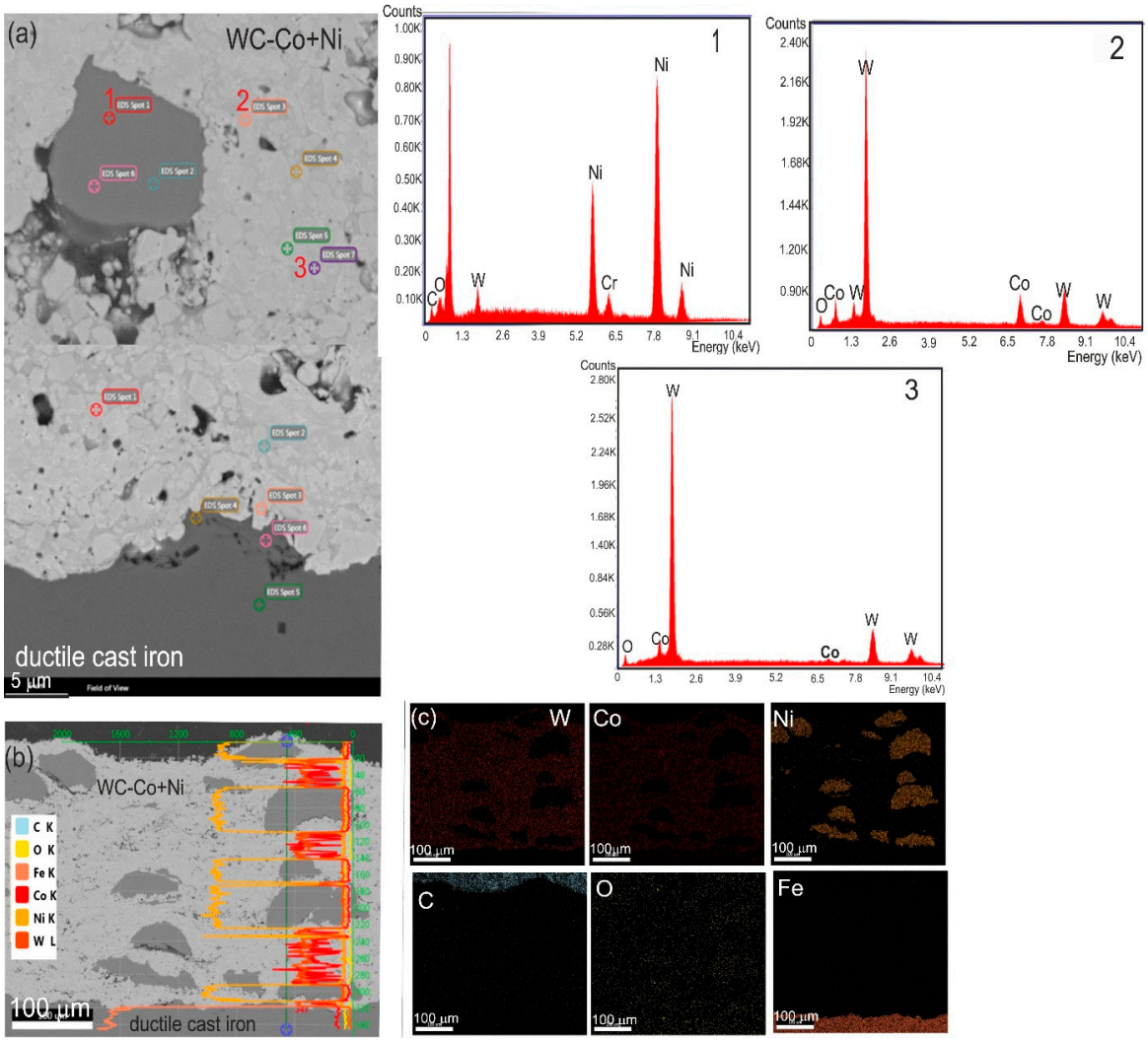

Figure 6. (a) Cross-sectional SEM images of the composite (WC-Co+Ni) coating with EDS spectra taken from the marked points 1,2, and 3: (b) linear representation of concentrations of C, O, Fe, Co, Ni,and W; (C) mapping the distribution of W, Co, Ni, C, O, Fe taken from the region of interface.

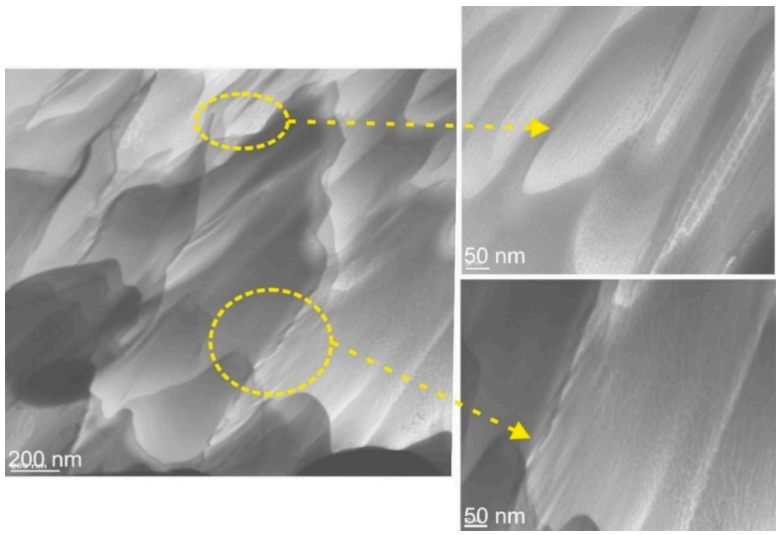

Figure 7. TEM image of the composite (WC-Co+Ni) coating deposited on ductile cast iron.

 doi:10.20944/preprints202604.0209.v1

X-ray diffraction (XRD) analysis of the WC–12Co coating modified with 10 wt.% Ni revealed that tungsten carbide (WC) remains the dominant phase (76.5%) (Figure 8). This indicates that the primary strengthening phase was effectively preserved during the HVOF spraying process and that degradation of the feedstock powder was limited. This is particularly important from the perspective of functional properties, as WC is characterized by very high hardness (HV ≈ 20–24 GPa), which governs its excellent resistance to abrasive wear, while exhibiting relatively low fracture toughness (K_{IC} ≈ 3–5 MPa·m$^{1/2}$). The presence of the W_2C phase (7.4%) indicates partial decarburization of WC during spraying. However, its content below 10% suggests that this process was controlled and did not lead to significant deterioration of coating properties. It should be noted that W_2C exhibits lower fracture toughness (K_{IC} ≈ 2–4 MPa·m$^{1/2}$), and higher fractions may promote microcrack initiation. The presence of the η phase (Co_6W_6C, 3.8%) confirms the occurrence of local diffusion reactions between the carbide phase and the metallic matrix. This phase, recognized as brittle (K_{IC} ≈ 1.5–3 MPa·m$^{1/2}$), may reduce fracture resistance; however, its low fraction indicates that these transformations were limited and did not significantly affect the mechanical performance of the coating. The Ni phase content, at approximately 12% (slightly above the nominal 10 wt.%), can be attributed to changes in phase equilibrium during spraying, including partial carbon loss. Nickel, similarly to cobalt, acts as a ductile phase, enhancing the matrix's ability to accommodate and relax residual stresses. The metallic matrix exhibits relatively high fracture toughness (on the order of 40–100 MPa·m$^{1/2}$), which contributes to inhibiting crack propagation initiated in brittle carbide phases.. In the context of these results, it should be emphasized that the formation of decarburization products (W_2C and η phase) is inevitable in high-temperature processes; however, their limited fraction is of key importance. Additionally, the fine-grained and locally nanostructured morphology of the carbide phases may further promote crack deflection and energy dissipation. In summary, the obtained phase composition (WC – 76.5%, W_2C – 7.4%, Co_6W_6C – 3.8%, Ni – 12.3%) indicates a well-developed microstructure in which the hard WC phase dominates, with a moderate contribution of decarburization products. This configuration provides an effective balance between high hardness and resistance to brittle fracture, characteristic of high-quality (WC–Co+Ni) coatings deposited by the HVOF method.

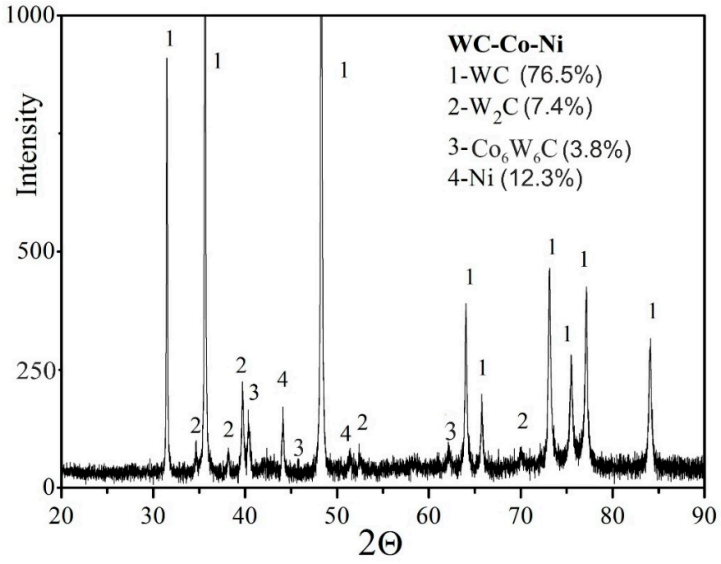

Figure 8. XRD pattern of the composite (WC-Co+Ni) coating.

Figure 9 shows the measurement location of surface roughness of the composite (WC–Co+Ni) coating, recorded using a laser confocal microscope at 200× magnification, together with a three-dimensional reconstruction of the surface topography. Analysis of the obtained images enabled a detailed assessment of the surface geometrical structure. The roughness parameters of the

 doi:10.20944/preprints202604.0209.v1

investigated coating were determined as R_a = 3.87 ± 0.14 μm and R_z = 14.40 ± 1.56 μm. The relatively high surface roughness is mainly associated with the composite nature of the coating and the presence of nickel particles, which appear as elongated, partially flattened features with an irregular, island-like distribution within the matrix. The presence of asperities of varying sizes contributes to increased surface development. An increase in the fraction and size of Ni particles leads to higher roughness, which should be considered when interpreting scratch test results, particularly in terms of adhesion and wear mechanisms. At the same time, such surface topography may enhance wear resistance through improved mechanical interlocking

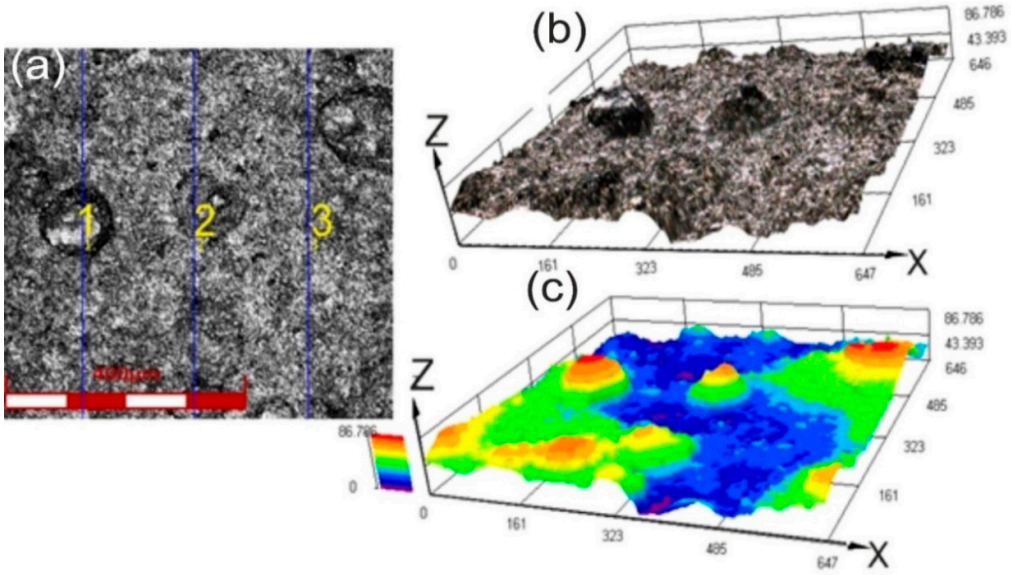

Figure 9. Surface morphology of the composite (WC–Co–Ni) coating on a cast iron substrate observed using a confocal microscope (200× magnification): (a) 2D intensity image, (b) 3D height reconstruction, (c) 3D color reconstruction.

3.2. Mechanical Characteristics of (WC-Co+N)i/Ductile Cast Iron System

The micromechanical properties, including indentation hardness (H_{IT}) and indentation Young's modulus (E_{IT}), determined on cross-sections of the (WC–Co+Ni)/ductile cast iron coating system, revealed significant variation with depth. The results summarized in Table 2 show that the average H_{IT} and E_{IT} values in the upper part of the coating are 10.05 ± 5.38 GPa and 244.78 ± 47.31 GPa, respectively. These values result from the coexistence of hard carbide phases and a ductile Ni-containing metallic phase within the microstructure. The observed variability is directly related to the heterogeneous lamellar structure of the coating and its phase composition (WC – 76.5%, W_2C – 7.4%, Co_6W_6C – 3.8%, Ni – 12.3%). The presence of Ni increases the fraction of the ductile phase, promoting a more uniform stress distribution and enhancing the ability to accommodate deformation, thereby stabilizing the mechanical response. The highest hardness and Young's modulus values were recorded in the central region of the coating (~100 μm from the substrate), which can be attributed to strain hardening during particle impact, improved interlamellar cohesion, and significant refinement of WC grains. The average H_{IT} values range from 9.39 to 14.23 GPa, with a maximum of 14.23 ± 3.85 GPa observed in regions enriched in hard phases. Locally elevated hardness values (up to ~18 GPa) correspond to indentations within WC particles, whereas lower values (~6–8 GPa) are characteristic of Co/Ni-rich regions. The variation in Young's modulus (E_{IT} ≈ 241–291 GPa) confirms the structural heterogeneity typical of HVOF-sprayed coatings. Secondary phases such as W_2C and Co_6W_6C locally increase stiffness and hardness, but may also enhance susceptibility to brittle deformation. In contrast, Ni-rich regions exhibit reduced hardness, lower stress concentration, and enhanced stress relaxation.

 doi:10.20944/preprints202604.0209.v1

The distribution of properties as a function of distance from the substrate indicates a general increase in hardness toward the coating surface. However, the absence of a clear monotonic trend suggests that the HVOF process ensured a relatively uniform phase distribution at the macroscopic scale, while local variations arise primarily from the lamellar structure and heterogeneous phase distribution. The largest scatter in H_{IT} values, observed in the coating–substrate interface region (±5.85 GPa), is attributed to residual stresses, local material mixing, diffusion effects, and partial decarburization and oxidation. The micromechanical response of the coating is governed by the interaction between hard carbide phases (WC, W_2C, Co_6W_6C) and a Co-based metallic matrix modified by Ni, which is present both in dissolved form and as partially unmolten ductile particles. The dominant WC fraction ensures high load-bearing capacity, while Ni stabilizes the mechanical response, reduces stress concentration, and limits local damage, which is critical for service performance. The H/E ratio, commonly used as an indicator of elastic strain resistance and contact deformation stability, reflects the load-bearing capacity and sliding stability of the WC–Co+Ni coating [37]. The highest H/E value (0.049) was obtained in line III, indicating enhanced resistance to crack initiation, whereas Ni-rich regions exhibited lower values, promoting stress redistribution and strain accommodation (Table 3). Similarly, the H^3/E^2 parameter, representing resistance to plastic deformation, reached its maximum in line III (0.034 GPa), consistent with the increased fraction of hard carbide phases.

Table 2. Indentation hardness (H_{IT}) and Young's modulus (E_{IT}) values of the (WC-Co+Ni)/ductile cast iron coating system.

Measuring Line	Region	H_{IT} [GPa]	E_{IT} [GPa]	Average H_{IT} [GPa]	Average E_{IT} [GPa]
I	Matrix (top)	13.28 13.03 3.83	288.83 295.27 150.23	10.05±5.38	244.78±47.31
II		11.57 7.83 8.76	266.13 250.58 241.38	9.39±1.95	252.69±12.51
III	Matrix (center)	10.52 18.21 13.95	238.69 332.52 301.78	14.23±3.85	290.99±47.85
IV	Matrix (bottom)	6.30 14.01 14.46	228.78 294.60 280.93	11.59±4.59	268.09±34.74
V	Interface	9.28 16.76 5.22	270.19 325.85 211.88	10.42±5.85	269.31±56.97

 doi:10.20944/preprints202604.0209.v1

Table 3. Indentation hardness, Young's modulus, and H/E and H^3/E^2 ratios of the composite (WC–Co+Ni) coating.

Measuring Line	Average H_{IT} [GPa]	Average E_{IT} [GPa]	H/E	H^3/E^2
I (top)	10.05	244.78	0.041	0.017
II (center)	9.36	252.69	0.037	0.013
III (center)	14.23	290.99	0.049	0.034
IV (bottom)	11.59	268.09	0.043	0.022
V (interface)	10.42	269.31	0.039	0.016

Fracture toughness (K_{IC}) results of the (WC–Co+Ni) coatings, presented in Table 4 together with representative indentation imprints, were evaluated based on indentation-induced crack lengths and impression diagonals using established indentation fracture mechanics models. The calculations were performed using the measured hardness (H_{IT}) and elastic modulus (E_{IT}) values. The results indicate that both hardness and Young's modulus play a significant role in governing fracture resistance. The highest K_{IC} values were recorded in matrix-dominated regions of the coating, whereas locally reduced values were observed in Ni-enriched areas. The presence of Ni, acting as a ductile phase relative to brittle WC carbides, promotes plastic deformation and suppresses crack propagation. As a result, the (WC–Co+Ni) coatings combine high hardness with enhanced plastic deformability, leading to improved resistance to wear and cracking. Higher K_{IC} values were obtained at lower loads (10–15 N), which is attributed to shorter crack lengths and a favorable E/H ratio that promotes plastic accommodation. The increased scatter of K_{IC} values in Ni-rich regions reflects the heterogeneous microstructure and local variations in mechanical properties. Furthermore, HVOF spraying has been reported to induce partial decarburization of WC particles and the formation of refined or locally nanocrystalline matrix regions, which may contribute to improved fracture resistance. Overall, the combined analysis of K_{IC}, H_{IT}, and E_{IT} confirms that local reductions in hardness in Ni-enriched regions enhance plastic deformability and suppress crack initiation, resulting in improved resistance to wear and fracture under tribological loading conditions.

Figure 10 shows the results of the four-point bending test for the WC–Co+Ni/ductile cast iron system, presented as the relationship between bending stress and deflection. The maximum bending stress for the WC–Co+Ni coating reached 1097 MPa at a deflection of 0.86 mm, whereas for the uncoated ductile cast iron the corresponding values were 1272 MPa and 1.12 mm, respectively. Despite the slightly lower deflection, the coated system maintains a high load-bearing capacity under bending, indicating efficient stress transfer and redistribution at the coating–substrate interface. The presence of a fine-grained metallic matrix and partially melted, ductile Ni particles leads to a local reduction in the effective Young's modulus and promotes stress relaxation. Under bending conditions, these Ni-rich regions act as local plastic deformation zones, reducing stress concentration at phase boundaries and limiting microcrack initiation.

 doi:10.20944/preprints202604.0209.v1

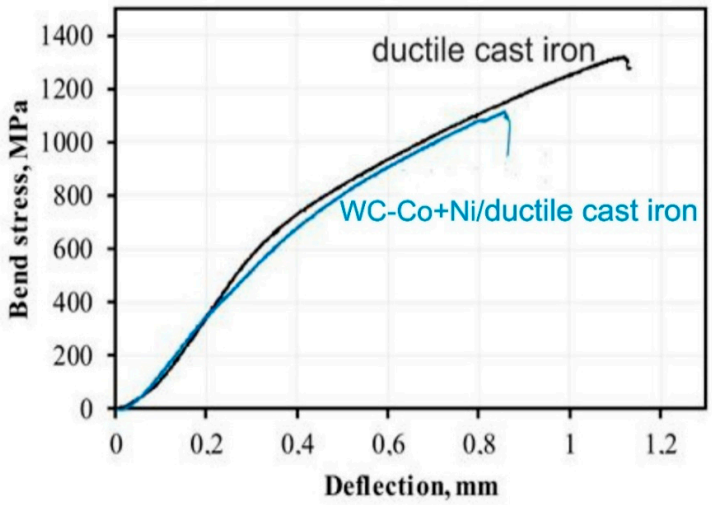

Figure 10. Bend test curves recorded for (WC-Co+Ni)/ductile cast iron system and ductile cast iron.

Table 4. Indentation fracture toughness measurements of the composite (WC-Co+Ni) coating under loads of 10, 15, 20, 25 and 30 N.

Load	H_{IT}= 4.92 GPa, E_{IT}= 189.92 GPa	H_{IT}= 12.18 GPa, E_{IT}= 250.03 GPa	H_{IT}= 5.32 GPa, E_{IT}= 198.97GPa
10N	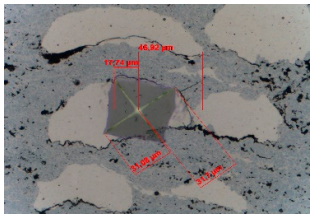	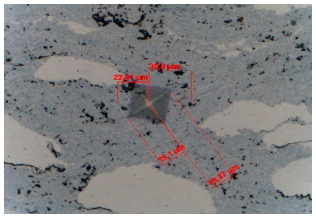	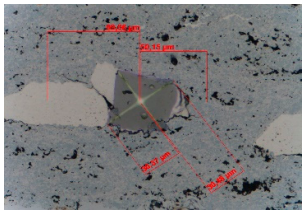
	K_{IC}= 3.71 [MNm$^{-3/2}$]	K_{IC}= 1.00 [MNm$^{-3/2}$]	K_{IC}= 1.41 [MNm$^{-3/2}$]
	H_{IT}= 14.05 GPa, E_{IT}= 260.21 GPa	H_{IT}=9.57 GPa, E_{IT}= 234.46 GPa	H_{IT}= 4.34 GPa, E_{IT}= 167.05 GPa
15N	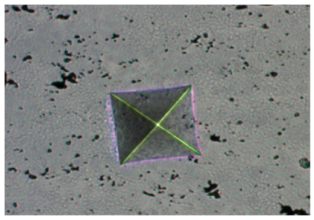	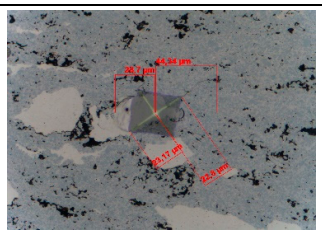	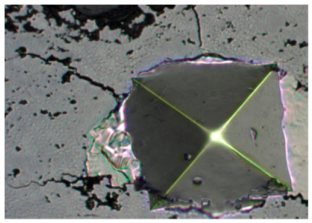
	no crack	K_{IC}= 2.15[MNm$^{-3/2}$]	no crack
	H_{IT}= 12.50 GPa, E_{IT}= 226.04 GPa	H_{IT}= 10.10 GPa, E_{IT}= 266.39 GPa	H_{IT}= 16.45 GPa, E_{IT}= 184.7 GPa
20N	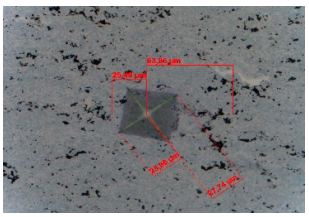	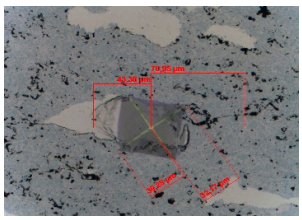	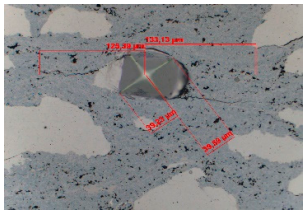
	K_{IC} = 1.59 [MNm$^{-3/2}$]	K_{IC}= 1.43 [MNm$^{-3/2}$]	K_{IC} = 0.76 [MNm$^{-3/2}$]
	H_{IT}= 12.90 GPa, E_{IT}= 211.04 GPa	H_{IT}= 10.34 GPa, E_{IT}= 214.42 GPa	H_{IT}= 5.87 GPa, E_{IT}= 178.08 GPa

 doi:10.20944/preprints202604.0209.v1

25N	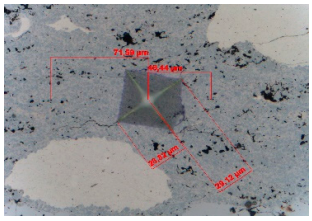	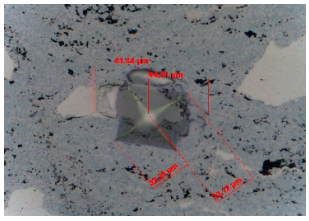	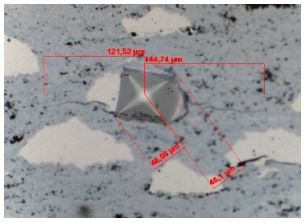
	K_{IC}= 1.61 [MNm$^{-3/2}$]	K_{IC}= 2.68 [MNm$^{-3/2}$]	K_{IC}= 0.84 [MNm$^{-3/2}$]
	H_{IT}= 11.21 GPa, E_{IT}= 212.57 GPa	H_{IT}= 5.81 GPa, E_{IT}= 159.32 GPa	H_{IT}= 5.59 GPa, E_{IT}= 161.8 GPa
30 N	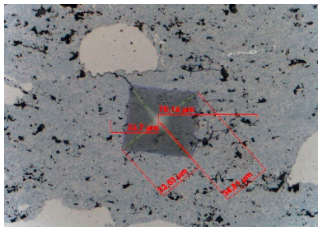	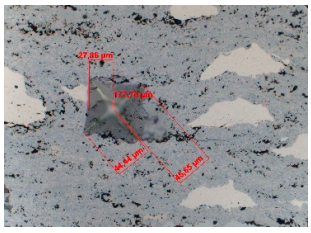	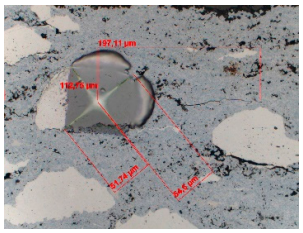
	K_{IC}= 1.96 [MNm$^{-3/2}$]	K_{IC}= 0.76 [MNm$^{-3/2}$]	K_{IC}= 0.65 [MNm$^{-3/2}$]

At the same time, they promote crack-bridging mechanisms, increasing the energy required for crack propagation. As a result, the coating exhibits high resistance to failure under bending conditions. Fractographic analysis after bending (Figure 11) confirms these observations. Cracks are observed to develop primarily within the coating and locally in the vicinity of the coating–substrate interface, without propagating into the ductile cast iron substrate. The presence of partially molten Ni particles acts as a local mechanical buffer, hindering crack growth and increasing resistance to crack propagation toward the substrate. This mechanism promotes effective dissipation of fracture energy within the coating and reduces stress transmission to the substrate. Consequently, the coating not only efficiently carries the applied load but also protects the substrate from excessive stress concentration, which is consistent with the observed high integrity of the coating–substrate interface. No signs of interfacial delamination were detected. In the analyzed system, differences in the coefficients of thermal expansion between the constituent phases and the substrate play a key role in the residual stress state. WC–Co-based coatings are characterized by a relatively low coefficient of thermal expansion (≈5–6 × 10^{-6} K^{-1}), significantly lower than that of the iron-based substrate (~13.2 × 10^{-6} K^{-1}). This mismatch promotes the development of compressive residual stresses in the coating during cooling, which may enhance resistance to crack initiation but requires partial stress accommodation to maintain adhesion. The introduction of Ni particles, with a coefficient of thermal expansion close to that of the substrate (~13 × 10^{-6} K^{-1}), partially compensates for this mismatch, reducing thermal strain gradients and limiting stress concentration within the coating microstructure. As a result, the WC–Co+Ni/ductile cast iron system exhibits high structural integrity, with no evidence of interfacial delamination, indicating that the residual stress level remains below the critical threshold for coating failure. The relatively similar elastic modulus values of the coating (E_{IT} ≈ 240–290 GPa) and the substrate (E ≈ 165 GPa for ductile cast iron) contribute to a reduced elastic mismatch, which may alleviate stress concentration in the interfacial region and promote more efficient load transfer across the coating–substrate interface. Fracture observations after bending tests reveal a mixed failure mode, consisting of cohesive fracture within the coating and localized interfacial cracking, confirming good interfacial adhesion and the absence of a dominant delamination mechanism. These observations are consistent with the analysis of the H/E and H^3/E^2 ratios, which indicate a balanced combination of hardness and elastic strain accommodation capability. In particular, the H/E ratio is associated with resistance to elastic deformation and crack initiation, whereas the H^3/E^2 parameter is related to resistance to plastic deformation. Together, these parameters suggest improved damage tolerance under mechanical and tribological loading conditions [36].

 doi:10.20944/preprints202604.0209.v1

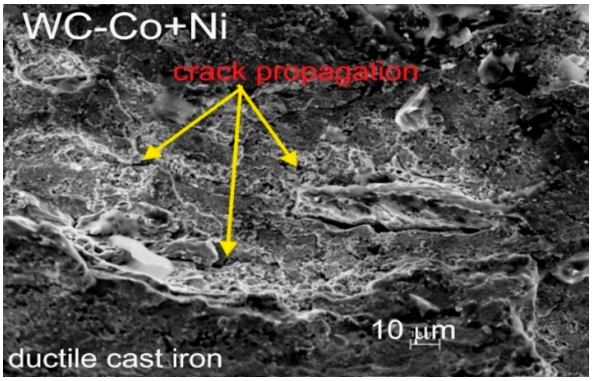

Figure 11. SEM micrograph of the fracture surface of the (WC-Co+Ni)/ductile cast iron system after bend test.

3.3. Tribological Characteristics of (WC-Co+Ni)/Ductile Cast Iron System

Figure 12 shows the variation of the cone crack area (Acn) for two scratch lengths (1.2 mm and 2.4 mm) as a function of the applied load. At the lowest load (5 N), only the onset of damage is observed, without the formation of a fully developed cone crack. In both cases, Acn increases systematically with increasing load up to 20 N, reaching a maximum value of 37.74 × 10^{-3} mm^2, indicating progressive cone crack propagation. This trend is confirmed by the micrographs in Figure 12, where well-developed cone fracture features are clearly visible in the load range of 15–20 N. Comparative analysis reveals that scratch length significantly influences the stability of cone crack evolution (Table 5). For the longer scratch length (2.4 mm), Acn exhibits a more regular, near-monotonic increase, suggesting a more stable stress distribution and more uniform crack propagation. In contrast, the shorter scratch length (1.2 mm) shows greater variability in Acn, which may be associated with localized stress fluctuations and increased sensitivity to microstructural heterogeneity. At 25 N, a deviation from the increasing trend is observed for both configurations, manifested either as a reduction in Acn (1.2 mm) or a deviation from monotonic growth (2.4 mm), suggesting a limitation in cone crack growth and a transition in the dominant damage mechanism. Microstructural observations (Figure 12) support this interpretation, as more complex damage morphologies, including cohesive cracking within the coating, become evident at the highest load. This behavior can be attributed to additional microstructural mechanisms associated with the presence of Ni particles, which may act as barriers to crack propagation through crack deflection and crack bridging. These mechanisms promote local energy dissipation and contribute to stabilization of cone crack growth. This effect is more pronounced for the longer scratch length, where a larger deformation volume enables averaging of local microstructural interactions. Overall, the results indicate that scratch length influences not only the magnitude of Acn but also the kinetics and stability of cone crack propagation, while the presence of Ni modifies the damage evolution and failure mechanisms, as reflected in the observed fracture morphology in Figure 12.

Table 5. Averaged scratch bond test results of the (WC-Co+Ni)/ductile cast iron system.

Scratch Length	Load [N]	Lx [µm]	Ly [µm]	A_{cn} x10^{-3} [mm^2]
1.2 mm	10	151.74	104.41	15.84
	15	108.86	152.68	16.62
	20	205.76	183.42	37.74
	25	115.51	259.56	29.98
2.4 mm	10	112.47	138.13	15.54
	15	127.50	201.98	25.64
	20	162.92	170.41	27.76
	25	170.71	198.34	33.86

 doi:10.20944/preprints202604.0209.v1

The morphology and composition of the wear track on the (WC–Co+N)i coating were analyzed using SEM/EDS (Figure 13) together with the wear depth profile (Figure 14). The worn surface exhibits a heterogeneous morphology with grooves, pull-out craters, and compacted debris, indicating predominantly abrasive wear. EDS analysis reveals a non-uniform elemental distribution, where W- and C-rich regions correspond to WC/W_2C fragments, while Co and Ni are associated with the metallic matrix. The presence of oxygen suggests tribo-oxidation, whereas aluminium originates from the Al_2O_3 counterbody, indicating material transfer. The wear depth profile shows a quasi-monotonic, step-like increase with wear distance, reflecting progressive material removal with local discontinuities related to carbide and carbide–matrix detachment. These fragments may act as loose abrasives, contributing to a three-body wear mechanism. The absence of abrupt depth increases indicates stable wear without dominant delamination. Overall, wear behavior is governed by microstructural heterogeneity and carbide–matrix cohesion, with Ni contributing to stabilization of the wear process by reducing stress concentration and limiting severe particle detachment.

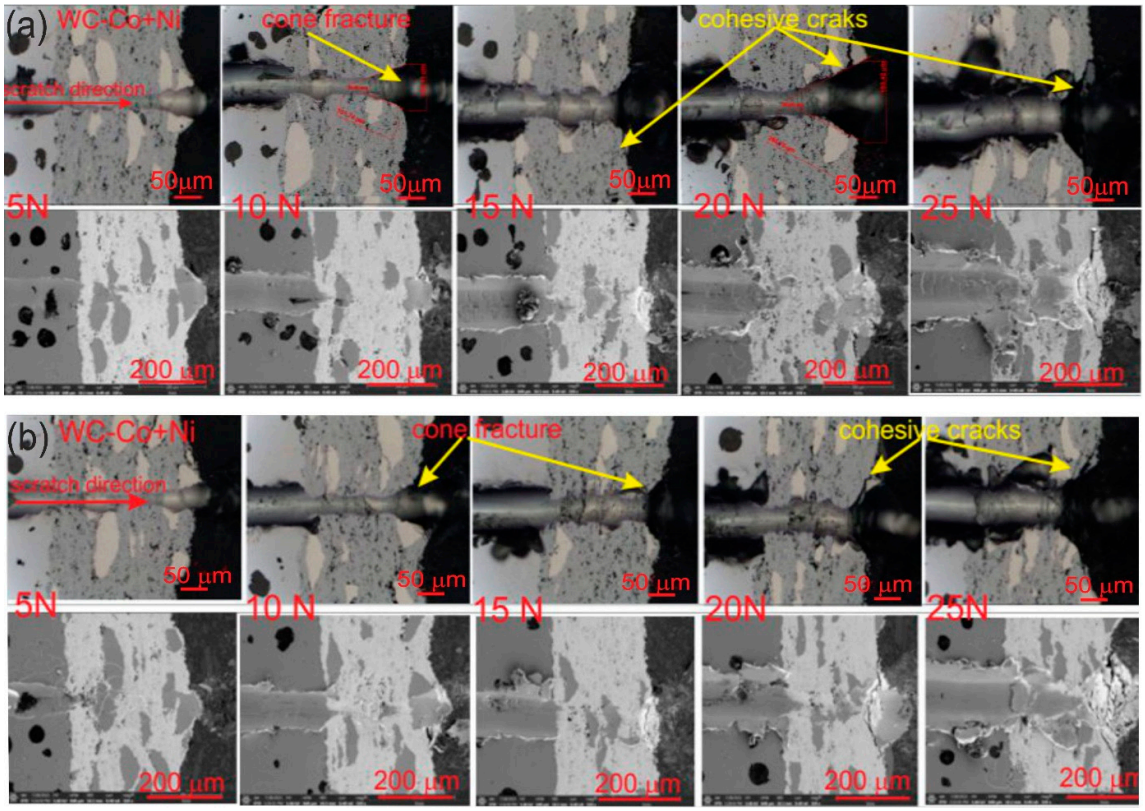

Figure 12. LM/SEM micrographs of damage evolution during the scratch bond strength test of the (WC–Co+Ni)/ductile cast iron system at increasing loads (5–25 N) for scratch lengths: (a) 1.2 mm and (b) 2.4 mm. The transition from initial damage to cone fracture (*cone fracture*, 15–20 N) and cohesive cracking (*cohesive cracks*, 25 N) is observed; scratch direction indicated.

 doi:10.20944/preprints202604.0209.v1

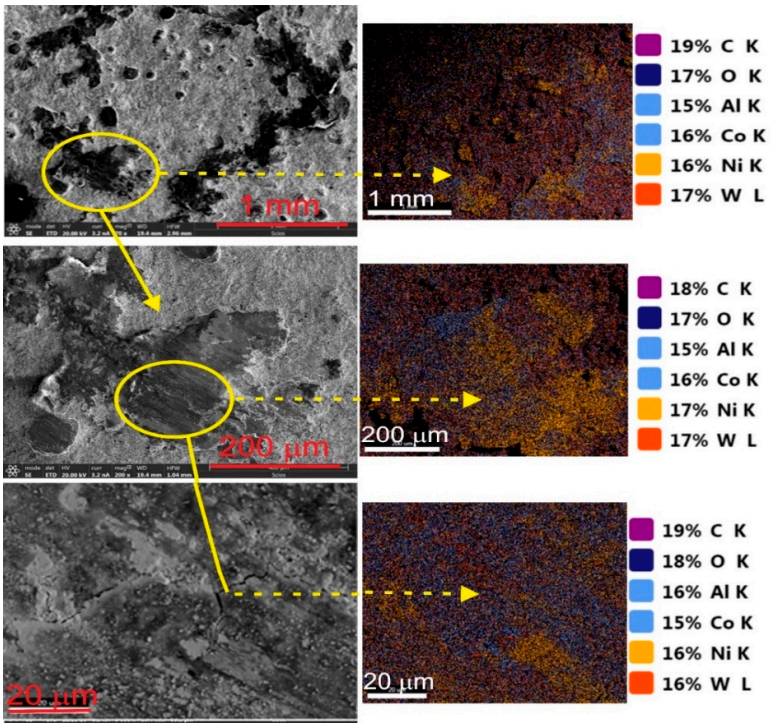

Figure 13. SEM images showing the wear morphology of the composite(WC-Co+Ni) coating along with the corresponding elemental maps.

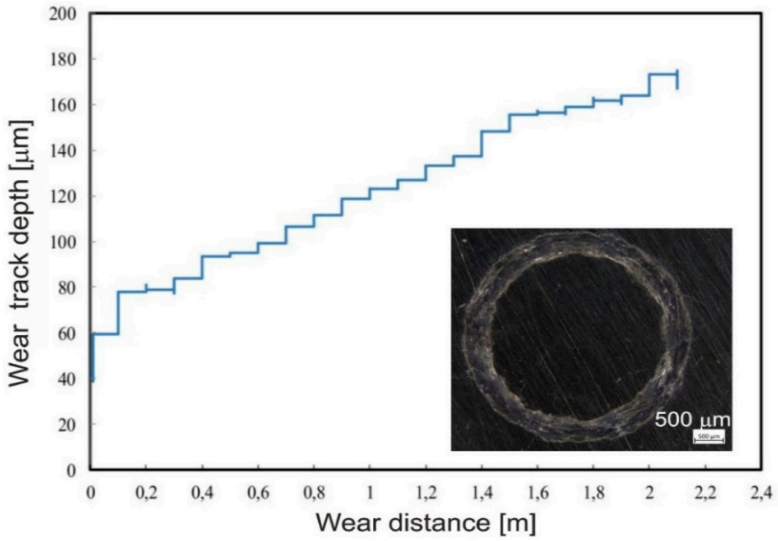

Figure 14. Dependence of the wear track depth of the WC-Co+Ni coating on the wear distance.

4. Conclusions

From the research conducted and the analysis of the results, the following conclusions can be drawn:

1. The composite (WC–Co+Ni) coating deposited using the HVOF technique exhibits a dense, low-porosity microstructure with a well-developed and defect-free interface between the coating and the ductile cast iron substrate. The coating is characterized by a heterogeneous structure consisting of a dominant WC phase embedded in a cobalt-based metallic matrix, additionally

 doi:10.20944/preprints202604.0209.v1

modified by nickel in the form of elongated, plastically deformed particles as well as partially molten, flattened Ni particles.

2. Phase analysis confirms that nickel is partially dissolved in the Co-based binder and partially retained as a distinct metallic phase, which enhances the structural heterogeneity of the coating. This dual nature of Ni contributes to improved microstructural cohesion and promotes effective stress redistribution within the composite structure. As a result, the coating demonstrates increased resistance to crack initiation and propagation, as well as stable load-bearing behavior without signs of interfacial delamination.
3. The modification of the coating composition through the addition of nickel significantly improves its mechanical and tribological performance. The presence of Ni reduces stress concentration in the carbide–matrix system, limits carbide pull-out, and enhances plastic deformation capability of the metallic matrix, which together contribute to improved structural integrity and damage tolerance of the coating.
4. The tribological behavior of the (WC–Co+Ni) coating is primarily governed by the integrity of the carbide–matrix system, where hard WC particles provide wear resistance, while the Co-based matrix ensures load transfer and cohesion. Nickel plays a key role in stabilizing wear mechanisms by promoting controlled material removal and reducing the severity of abrasive interactions.
5. (WC–Co+Ni) coatings deposited on ductile cast iron substrates by the HVOF process represent an effective solution for applications requiring high load-bearing capacity, enhanced wear resistance, and improved structural stability under mechanical loading. The synergistic interaction between hard WC particles, the Co-based binder, and nickel modification ensures balanced mechanical performance and reliable operational behavior in demanding service conditions.

Author Contributions: Conceptualization, M.K.; Methodology, M.K. L.B. and A.T.; Investigation, M.K. L.B. and A.T.; Formal analysis, M.K. L.B. and A.T.; Writing- original draft preparation, M.K.; Writing- review and ending, M.K.; Visualization, M.K. A.T and L.B; All authors have read and agreed to the published version of the manuscript.

Funding: This research was funded by subsidy of the Department of Non-Ferrous Metals of AGH University of Krakow (contract No. 501.00 180 000).

References

1. Stewart, D.A.; Shipway, P.H.; McCartney, D.G. Microstructural evolution in HVOF sprayed WC–Co Coatings. *Acta Mater.* **2000**, *48*, 1593–1604
2. Shipway, P.H.; Hogg, J.J. Abrasive wear behaviour of HVOF sprayed WC–Co coatings. *Wear.* **2005**, *259*, 44–51
3. Murthy, J.K.N.; Venkataraman, B. Abrasive wear behaviour of WC–CoCr coatings deposited by HVOF spraying. Surf.& Coat. Technol. **2006**, 200, 2642–2652
4. Guilemany, J.M.; Fernández, J.; Miguel, J.M. Tribological behaviour of WC–Co coatings. *Tribol.* Interna. **2002**, 35, 567–575
5. Suhonen, T.; Varis, T.; Turunen, E. Tribology of HVOF and HVAF sprayed WC-10Co4Cr coatings, Surf.& Coat. Technol. **2015**, 265, 125–144
6. Lima, R.S.; Marple, B.R. Nanostructured WC–Co coatings produced by thermal spraying. *J. Thermal* Spray Technol. **2007**, 16, 40–63
7. Chivavibul, P.; Watanabe, M.; Kuroda, S. Microstructure and mechanical properties of WC–Co coatings deposited by HVOF spraying. *Surf.& Coat. Technol.* **2007**, *202*, 509–521
8. Sampath, S.; Wayne, S.F. Processing–structure relationships in thermal spray coatings. *J. Thermal* Spray Technol.**1994**, 3, 307–317
9. Li, C.J.; Yang, H. Formation mechanisms of HVOF sprayed WC–Co coatings. *Mater.& Manufact.* Process. **1999**, 14, 383–394

 doi:10.20944/preprints202604.0209.v1

10. Kleis, I.; Berger, L.-M.; Zieris, R.; Jaworski, A. Microstructure and properties of HVOF-sprayed chromium alloyed WC–Co and WC–Ni coatings. *Surf. Coat. Technol*. **2008**, *202*, 4417–4421
11. Yin, A.S.Y.N.; Kamdi, Z.; Ainun, R.; Hussin, R.; Siti Aida, I. Tungsten carbide–nickel (WC–Ni) coating as potential wear and corrosion protection for metal. *Mater. Sci. Forum*. **2020**, *1010* 286–291
12. Harish, U.; Mruthunjaya, M.; Chakule, R. R.; Aswar, S. J.; Durga Prasad, C.; Balaji, S.; Nandakumar, M. B.; Jayasheel Kumar, K. A.; Aden, Adem Abdirkadir. Effect of cobalt variation on microstructural and erosion performance of HVOF-sprayed WC–Co–Cr–Ni hard-faced coatings. J. Mater. Sci.: Mater. Electron. **2025**, 20, 73 (article numer)
13. Wang, Y.; Wang, H.; Zhao, Z.; Hou, C.; Liu, X.; Song, X. Wear and corrosion resistant HVOF-sprayed WC-xCr_3C_2-8Co-6Ni coatings produced from pre-alloyed powder. *Surf.& Coat. Technol.* **2023**, *473*, 129989
14. Wang, X.-Z.; Wang, H.-B.; Liu, X.-M; Yang, T.; Song, X.-Y. Grain growth inhibitor on the WC–Co cemented carbide coating. *J. Inorg. Mater*. **2017**, *32(8)*, 813–818
15. Yao, J.; Liu, F.; Tan, L.; Huang, L.; Liu, Y. Decarburization control and performance enhancement: optimizing HVOF sprayed submicron WC-12Co coating with additives. *Int. J.* Refract. Metals Hard Mater. **2024**, 124, 106846
16. Zhu, Z.-W.; Chen, Q.-Y.; Bai, X.-B.; Yang, C.; Ji, G.-C.; Zhang, M.-X.; Wang, H.-T.; Yao, H.-L.; Wang, F. Microstructure, phase constitution and mechanical properties of WC-Cr_3C_2-CoNiLa coatings fabricated by using HVOF spraying core-shell powder. *Int. J. Refract. Metals Hard Mater.* **2022**, *106*, 106862
17. Pawlowski, J. The Science and Engineering of Thermal Spray Coatings, 2nd ed., Wiley, Chichester, 2008
18. Murthy, H.; Venkataraman, B. Sliding wear behavior of HVOF sprayed WC–Co coatings. *Wear*. **2001**, *249*, 592–600
19. Matthews, S.; James, B. Review of thermal spray coatings for protection against wear. *Surf. Coat. Technol*. **2009**, *203*, 1086–1093
20. Hussain, T.; McCartney, A.; Shipway,P.; Zhang, D. A review of HVOF thermal sprayed coatings for wear resistance. *J. Therm. Spray Technol*. **2007**, *16*, 1–16
21. Babu, M.; Basu, B.; Sundararajan, G. Processing–microstructure–wear relationship in WC–Co coatings. *Acta Material*. **2008**, *56*, 5012–5026
22. Myalska, H.; Moskal, G. Microstructure of WC-Co coatings produced by HVOF spraying, *Solid* State Phenom. **2015**, 226, 149–156
23. Wang, W.; Ji, G.; Chen, Q. Microstructure characterization and abrasive wear performance of HVOF sprayed WC-Co coatings. *Advanced Mater. Research.* **2011**, *189–193*, 707–710
24. Mateen, A.; Khalid, F.A.; Khan, T.I. Wear behaviour of HVOF sprayed WC-Co coatings. *Advanced* Mater. Research. **2011**, 326, 144–150
25. Suhonen, T.; Varis, T.; Turunen, E. Effect of microstructure on mechanical properties of HVOF sprayed WC-CoCr coatings. Tribologia – Finnish Journal of Tribology. **2009**, 28, 14–28
26. Żórawski W.; et al. Microstructure and tribological properties of HVOF-sprayed nanostructured WC-12Co coatings. *Coatings* **2024,** *14*, 752
27. Mruthunjaya, M.; Parashivamurthy K.I. Microstructural study and tribological behavior of WC-Co coatings produced by HVOF, *Interna. J. Mechan. Engin.& Technol.* **2014**, *5*, 132–139
28. S. Lay, S.; S. Hamar-Thibault, S.; G. Béranger G. VC- and Cr_3C_2-doped WC–NbC–Co hardmetals J. Alloys and Compoun. **2008**, 457 (1–2), 263–267
29. Yin, C.; Peng, Y.; Ruan, J.; Zhao, L.; Zhang, R.; Du, Y. Influence of Cr_3C_2 and VC Content on WC Grain Size, WC Shape and Mechanical Properties of WC–6 wt.% Co Cemented Carbides. *Materials*, **2021**, 14 (6), 1551 (article number)
30. Liu, X.; et al. Influence of VC and Cr_3C_2 as grain growth inhibitors on WC–Al_2O_3 composites prepared by hot press sintering. *Internat. J. Refrac. Metals & Hard Mater.* **2014**, *43*, 211–217
31. Lima, R.S.; Marple, B.R. Thermal spray coatings engineered from nanostructured ceramic agglomerated powders for structural, thermal barrier and biomedical applications: A review. *J.* Thermal Spray Technol. **2007**, 16, 40–63

 doi:10.20944/preprints202604.0209.v1

32. Wang, D.;: Zhang, B.; Jia, Ch.; Gao ,F.; Yu, Y.; Chu, K.; Zhang, M.; Zhao, X.; Liang, X. Influence of carbide grain size and crystal characteristics on the microstructure and mechanical properties of HVOF-sprayed WC–CoCr coatings. *Int. J. Refract. Met. Hard Mater*. **2017**, *69*, 138–152
33. de Hosson, A.R.; Budinski, K.G. Tribology of WC–Co coatings: role of tribo-oxidation and formation of protective tribofilms. *Surf.& Coat. Technol.* **2006**, *201*, 203–211
34. Strecker, A.; Salzberger, U.; Mayer, J. Specimen preparation for transmission electron microscopy: reliable method for cross-sections and brittle materials. *Prakt. Metallogr*. **1993**, *30*, 482-495
35. Anstis, G.R.; Chantikul, P.; Lawn, B.R.; Marshall, D.B. A critical evaluation of indentation techniques for measuring fracture toughness: I, Direct crack measurements. *J. Amer. Ceram. Soc.* **1981**, *64*, 533-538
36. ISO 27307:2015 Thermal spraying — Evaluation of adhesion/cohesion of thermal sprayed ceramic coatings by transverse scratch testing; ISO International Standards: 2015.
37. Leyland, A.; Matthews, A. On the significance of the H/E ratio in wear control: a nanocomposite coating approach to optimised tribological behaviour. *Wear*. **2000**, *246*, 1–11.